
HiFuse: HIERARCHICAL MULTI-SCALE FEATURE FUSION NETWORK FOR MEDICAL IMAGE CLASSIFICATION

A PREPRINT

Xiangzuo Huo*

Xinjiang University
huoxiangzuo@163.com

Gang Sun*

The Affiliated Cancer Hospital of
Xinjiang Medical University
sung853219@163.com

Shengwei Tian†

Xinjiang University
tianshengwei@163.com

Yan Wang†

The Affiliated Cancer Hospital of
Xinjiang Medical University

Long Yu

Xinjiang University

Jun Long

Central South University

Wendong Zhang

Xinjiang University

Aolun Li

Xinjiang University

September 22, 2022

ABSTRACT

Medical image classification has developed rapidly under the impetus of the convolutional neural network (CNN). Due to the fixed size of the receptive field of the convolution kernel, it is difficult to capture the global features of medical images. Although the self-attention-based Transformer can model long-range dependencies, it has high computational complexity and lacks local inductive bias. Much research has demonstrated that global and local features are crucial for image classification. However, medical images have a lot of noisy, scattered features, intra-class variation, and inter-class similarities. This paper proposes a three-branch hierarchical multi-scale feature fusion network structure termed as HiFuse for medical image classification as a new method. It can fuse the advantages of Transformer and CNN from multi-scale hierarchies without destroying the respective modeling so as to improve the classification accuracy of various medical images. A parallel hierarchy of local and global feature blocks is designed to efficiently extract local features and global representations at various semantic scales, with the flexibility to model at different scales and linear computational complexity relevant to image size. Moreover, an adaptive hierarchical feature fusion block (HFF block) is designed to utilize the features obtained at different hierarchical levels comprehensively. The HFF block contains spatial attention, channel attention, residual inverted MLP, and shortcut to adaptively fuse semantic information between various scale features of each branch. The accuracy of our proposed model on the ISIC2018 dataset is 7.6% higher than baseline, 21.5% on the Covid-19 dataset, and 10.4% on the Kvasir dataset. Compared with other advanced models, the HiFuse model performs the best. Our code is open-source and available from <https://github.com/huoxiangzuo/HiFuse>.

Keywords Medical Image Classification · Feature Fusion · Swin Transformer · Hybrid Network · Multi-scale Feature

1 Introduction

Medical image classification is an important task in computer-aided diagnosis, medical image retrieval, and mining. In recent years, convolutional neural networks have achieved outstanding performances in many medical image

*Equal contribution

†Corresponding author

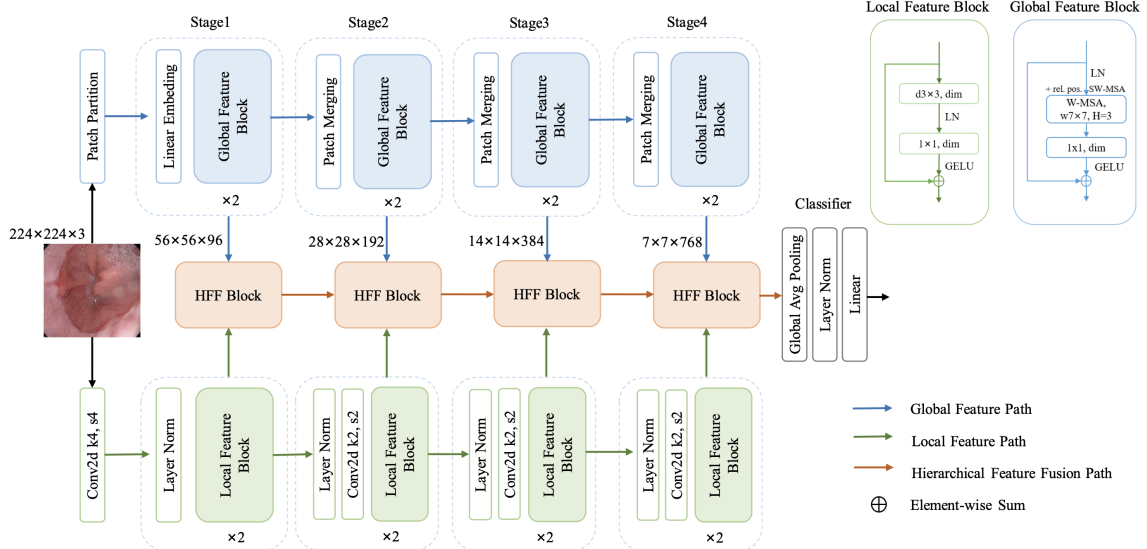


Figure 1: Overall structure of the HiFuse model.

classification tasksKoitka and Friedrich [2016], Xu et al. [2014], Shen et al. [2017], Esteva et al. [2017], Personnaz et al. [1986], Kumar et al. [2016], Yu et al. [2017]. However, medical images have high similarity and detail diversity in imaging modalities and clinicopathology, resulting in significant intra-class variation and inter-class similarity, requiring modeling of global semantic information, so medical image classification remains challenging.

TransformerVaswani et al. [2017] was originally used for modeling sequence-to-sequence prediction in natural language processing (NLP) tasks. Now Transformer has also attracted much attention in the computer vision community, ViTDoSovitskiy et al. [2020] by segmenting each image into patches with positional embeddings. Sequences of tokens are constructed, and a cascaded transformer block is applied to extract parameterized vectors as visual representations that model global semantic information through complex spatial transformations and long-range feature dependencies. Due to the lack of local spatial feature details. Li et al.Yuan et al. [2021] proposed to utilize CNN feature maps as input tokens to capture feature neighborhood information. However, they model the image as a one-dimensional sequence of tokens, ignoring the local inductive bias of the image, which affects the convergence speed and performance of the model.

Recent studies, such as ViTAEXu et al. [2021], StoHisNetFu et al. [2022], TransfuseZhang et al. [2021], CMTGuo et al. [2022a], ComformerPeng et al. [2021] and so on, which solve the above problems to a certain extent by Fusion of the features extracted by the convolution and self-attention mechanismVaswani et al. [2017]. Different from the above methods, to further exploit the advantages of CNN and Transformer in the medical field, a three-branch parallel hierarchical fusion network structure termed as HiFuse is proposed as a new method for medical image classification to improve the classification accuracy of various medical images. Taking ConvNextLiu et al. [2022] as our baseline and inspired by ResNetHe et al. [2016] and Swin TransformerLiu et al. [2021], we designed new local and global feature blocks. HFF blocks fuse local and global representations of various semantic scales. This fusion process can fully mine the deep-shallow and global-local features of the lesion area in the medical image classification task.

HiFuse has the following advantages:

1. Combining the advantages of CNN and Transformer, a parallel framework of Local and Global feature blocks is designed to efficiently capture local spatial context features and global semantic information representation of features at different scales, respectively. In addition, HiFuse does not need to build a very deep network to achieve good results, effectively avoiding the problems of gradient disappearance and loss of feature information.
2. An adaptive hierarchical feature fusion block (HFF block) is designed, which contains spatial attention, channel attention, residual inverted MLP, and shortcut connection to adaptively fuse semantic information between different scale features of each branch.
3. The proposed HiFuse model achieves relatively good results on ISIC2018, Covid-19, and Kvasir datasets.

2 Related Works

Traditional medical image classification methods employ color, texture, shape, and combined descriptors. Baloch et al. Baloch and Krim [2007] proposed a flexible skew-symmetric shape model to learn to capture latent changes within a certain neighborhood. Song et al. Song et al. [2013] proposed a novel texture descriptor that represents texture features by integrating multi-scale Gabor transform and local binarized histograms to classify lung tissue. Koitka et al. Koitka and Friedrich [2016] manually extracted visual descriptors and used them for medical image classification.

Medical image classification work based on deep learning has emerged in recent years. The deep convolutional neural network (DCNN) method that has greatly improved the classification accuracy and reduced the waste of resources for manual feature extraction is gradually applied clinical auxiliary diagnosis. Xu et al. Xu et al. [2014] used DCNN to extract features from histopathological images of colon cancer and achieved good classification results. Shen et al. Shen et al. [2017] proposed a multi-scale crop pooling strategy for DCNN to capture lung nodule classification features on chest CT images.

Esteva et al. Esteva et al. [2017] used a model trained on 129,450 clinical images to diagnose the most common and deadly skin cancers and achieved performance matching 21 dermatologists. Koitka et al. Koitka and Friedrich [2016] custom-train the output of the last fully connected layer in a pre-trained ResNet-152 model, illustrating that transfer learning can achieve good results in medical image classification. Kumar et al. Kumar et al. [2016] integrated two different pretrained DCNN architectures and combined them into a more powerful classifier. Cheng et al. Cheng et al. [2022] proposed a modular group attention block that captures feature correlations in medical images' channel and space dimensions. However, these models cannot collect sufficient contextual information, and global semantic information features are equally important in high-resolution medical images.

Transformer Vaswani et al. [2017] was originally used in NLP. It extracts intrinsic properties through a self-attention method. ViT Dosovitskiy et al. [2020], as a pioneer work, verifies the feasibility of pure Transformer architecture in computer vision tasks, and is gradually used for image classification Yuan et al. [2021], Wu et al. [2020], Touvron et al. [2021], object detection Carion et al. [2020], Zhu et al. [2020], Beal et al. [2020], semantic segmentation Zheng et al. [2021], Zhang et al. [2021], Gao et al. [2021], image enhancement Chen et al. [2021] and image generation Wan et al. [2021]. Researchers Valanarasu et al. [2021], He et al. [2021], Jiang et al. [2021], Wang et al. [2021] have tried various approaches to make transformers more successful in computer vision. However, the self-attention mechanism in the visual Transformer often ignores local feature details, and for weak local features, it is not easy to distinguish the object from the background.

To address the lack of local features, DeiT Touvron et al. [2021] proposed using distilled tokens to transfer the CNN-based features to the visual Transformer. T2TViT Yuan et al. [2021] proposed using a tokenization module recursively reorganizing images to consider adjacent pixels' tokens. The models, such as VitAE, StoHis, TransFuse, CMT, Conformer and so on, Xu et al. [2021], Fu et al. [2022], Zhang et al. [2021], Guo et al. [2022a], Peng et al. [2021] not only inherit the structural advantages of CNN and Transformer, but also verify that the coupling of local features and global representation can significantly enhance Transformer discriminability of weak local features. The above models perform well on natural datasets such as ImageNet and various downstream tasks, however, when applied to the medical image domain, the results are unsatisfactory. Because the datasets of medical images are insufficient, pathological features are more scattered and difficult to discover than those of ordinary images. So, we decide to take full advantage of deep-shallow and global-local features and a wider fusion network to fuse them. Our proposed HiFuse model defines a three-branch hierarchical parallel fusion structure, combines local with global feature blocks, and designs a hierarchical feature fusion block (HFF block) to fuse these features and keep local and global branches undisturbed. HiFuse inherits not only the advantages of CNN and Transformer but also local features and global representations that are coupled at different scales.

3 Proposed Method

3.1 Overview

The HiFuse model, as a new medical image classification method, is proposed to effectively obtain local spatial information and global semantic representations of medical images at different scales. We use a parallel structure to extract the global and local information of medical images from the global and local feature blocks, fusing the features of different hierarchies through the HFF block, downsampling step, and finally, obtaining the classification result. In the following sections, we first introduce the overall structure of the HiFuse model, then introduce the global feature block and the local feature block, respectively. We describe the details of the HFF block in Section 3.5.

Table 1: HiFuse specific parameters.

stage	output size	Local Branch		HFF Branch		Global Branch					
stem	56×56, 96	4×4, 96, stride 4		-		4×4, 96, stride 4					
1	56×56	d3×3, 96 1×1, 96	x2	→spatial attention	channel attention←	MSA, w7×7, head 3, rel. pos. SW-MSA 1×1, 96	x2				
				d3×3, 96 1×1, 384 1×1, 96							
2	28×28	d3×3, 192 1×1, 192	x2	→spatial attention	channel attention←	MSA, w7×7, head 6, rel. pos. SW-MSA 1×1, 192	x2				
				d3×3, 192 1×1, 768 1×1, 192							
3	14×14	d3×3, 384 1×1, 384	x2	→spatial attention	channel attention←	MSA, w7×7, head 12, rel. pos. SW-MSA 1×1, 384	x2				
				d3×3, 384 1×1, 1536 1×1, 384							
4	7×7	d3×3, 768 1×1, 768	x2	→spatial attention	channel attention←	MSA, w7×7, head 24, rel. pos. SW-MSA 1×1, 768	x2				
				d3×3, 768 1×1, 3072 1×1, 768							
Parameters		82.49 M									
FLOPs		8.13 G									

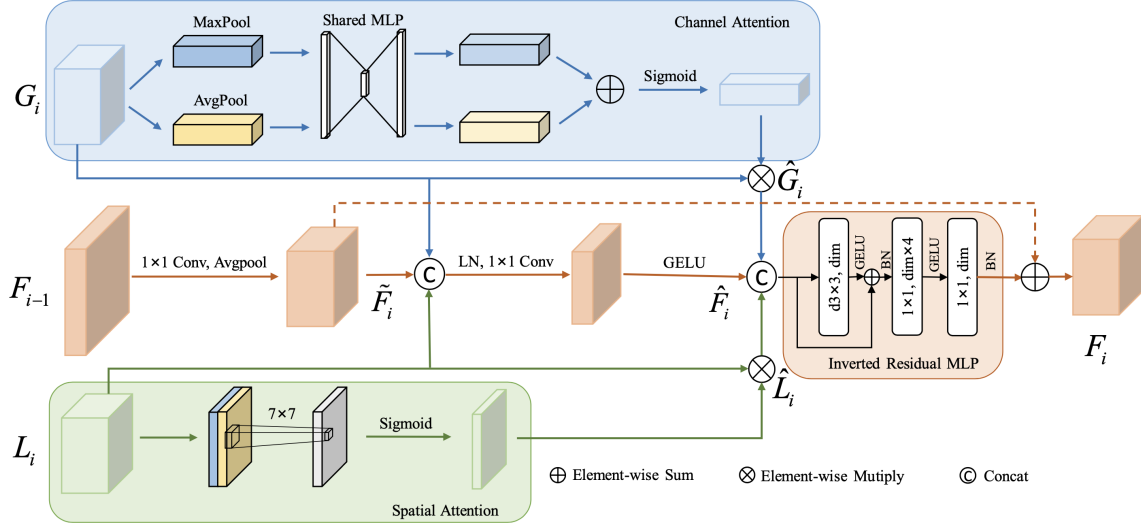


Figure 2: HFF block detail display.

3.2 The Multi-stage Design for HiFuse

In order to improve the accuracy of the classification model of medical images, it is necessary to fuse local features and global representations from different hierarchical levels. We designed a parallel network structure for hierarchical feature fusion. The overall structure of HiFuse is shown in Figure 1. The local branch is used to extract the local features of the image, and the global branch is used to extract the global semantic representation of the image. Both branches consist of 4 Stages for feature extraction at different scales. The stem block of the local branch is a 4×4 convolution with stride 4, followed by Layer Norm Carion et al. [2020]. The stem module of the global branch divides the image through the patch partition module. Each 4×4 adjacent pixel is a patch and then flattened in the channel direction. Patch merging changes the output to 2 times the input channel through the linear embedding layer and applies the global feature block for feature transformation. The specific parameters are shown in Table 1.

The three-branch parallel structure means that local features and global representations can be preserved to the greatest extent without interfering with each other. Feature maps of different hierarchical levels are constructed through four stages. HFF blocks are used to fuse each stage's local features and global representations and connect the output from the previous stage. The output of local features of each hierarchy of local through spatial attention is combined with the global features of each hierarchy of global through channel attentionWoo et al. [2018]. Finally, the combined features are fed to the linear classifiers of Global Average Pooling and Layer Norm for classification. We build different HiFuse variants, HiFuse-Tiny/Small/Base; these variants have different numbers of global and local feature blocks in each stage and build models with different depths to deal with datasets of various sizes. The hyper-parameters of these model variants are:

- HiFuse-Tiny: Block numbers = (2, 2, 2, 2)
- HiFuse-Small: Block numbers = (2, 2, 6, 2)
- HiFuse-Base: Block numbers = (2, 2, 18, 2)

3.3 Global Feature Block

The imaging methods and clinical pathology of medical images are diverse, with significant intra-class changes and inter-class similarities. The acquisition of global semantic information is very important. Therefore, we introduced the Windows Multi-head Self-Attention (W-MSA) in the global feature extraction branch. W-MSA is the Swin TransformerLiu et al. [2021] first proposed, Compared with the Multi-head Self-Attention (MSA) module in the Transformer, the W-MSA module, which can effectively reduce the amount of computation and divide the feature map into $M \times M$ sizes. Window one by one, and then perform self-attention on each Window individually. The computational complexity formula is shown in (1).

$$\begin{aligned}\Omega(\text{MSA}) &= 4hwC^2 + 2(hw)^2C \\ \Omega(\text{W-MSA}) &= 4hwC^2 + 2M^2hwC\end{aligned}\quad (1)$$

where h represents the height of the feature map, w represents the width of the feature map, C represents the depth of the feature map, and M represents the size of each window.

For each stage, by incorporating the patch into the global feature block, the feature map goes through LayerNorm Ba et al. [2016] layer into W-MSA and then through the linear layer with the GELU activation function, as shown in Figure 1. A residual connection is applied after each module, a relative position bias (rel. pos.) is used, and Shift W-MSA is introduced in the next module. This process is depicted in (2).

$$\begin{aligned}g_i &= f^{1 \times 1}(\text{W-MSA}(LN(G_{i-1}))) + G_{i-1} \\ G_i &= f^{1 \times 1}(\text{SW-MSA}(LN(g_i))) + g_i\end{aligned}\quad (2)$$

where G_i and g_i denote the output features of the Shift W-MSA and the W-MSA for the global feature block. $f^{1 \times 1}$ is the convolution operation with a convolution kernel size of 1×1 , which is equivalent to the linear operation. LN is the LayerNorm operation. Finally, the extracted global features are input into the HFF block.

3.4 Local Feature Block

Local spatial features in medical images are also very important. The local feature block, shown in Figure 1, uses a 3×3 depthwise convolution Howard et al. [2017], Chollet [2017], a special case of grouped convolutions Xie et al. [2017]; the number of groupings is equal to the number of channels. The use of depthwise convolutions effectively reduces the FLOPs of the network. And then, cross-channel information interaction through linear layers obtains good performance in different application scenarios by borrowing the LN and GELU activation functions in the Transformer. Finally, the extracted local features are input into the HFF block. This process is depicted in (3).

$$L_i = f^{1 \times 1}(LN(f^{d3 \times 3}(L_{i-1}))) + L_{i-1} \quad (3)$$

where L_i denote the output features of the local feature block. $f^{d3 \times 3}$ is the depthwise convolution operation with a convolution kernel size of 3×3 .

Macroscopically, local and global branch structures are similar, and the design of the same number of channels and hierarchical structure lays the foundation for fusing local and global encoding features of different scales. How to effectively fuse features of different scales in each branch becomes a new problem. To this end, we propose the HFF block.

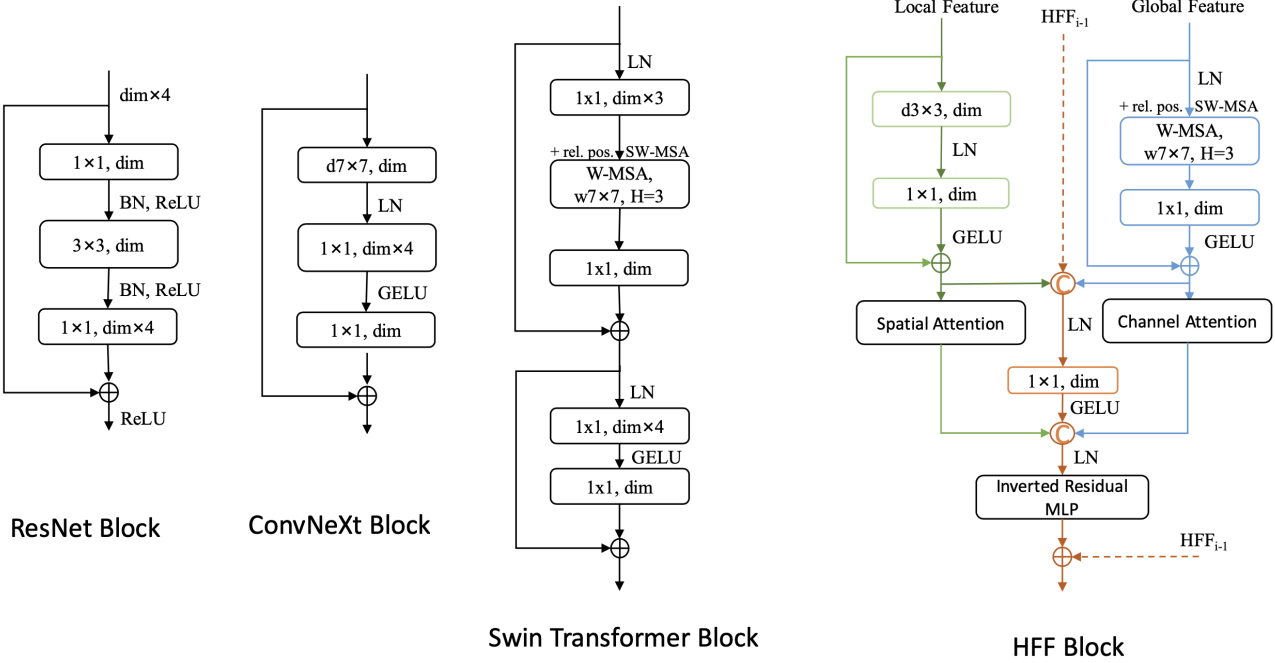


Figure 3: Block designs for a ResNet, a ConvNeXt, a Swin Transformer and a HFF.

3.5 HFF Block

Adaptive hierarchical feature fusion block can adaptively fuse local features from different layers, global representations, and semantic information after fusion from the previous hierarchy according to the input features, as shown in Figure 2. Among them, G_i represents the feature matrix output by the global feature block, L_i represents the feature matrix output by the local feature block, F_{i-1} represents the feature matrix output by the previous stage of HFF, and F_i represents the feature matrix generated by HFF fusion at this stage.

Since the self-attention in the global feature block can capture the spatial and temporal global information Guo et al. [2022b] to a certain extent, the HFF block feeds the incoming global features into the channel attention (CA) mechanism, which utilizes the interdependence between the channel maps to improve the feature representation of specific semantics. The local features are input into the spatial attention (SA) mechanism to enhance local details and suppress irrelevant regions. Finally, the results generated by each attention and the fusion path will be feature fusion, and a residual inverted MLP (IRMLP) will be connected. To a certain extent, the problems of gradient vanishing, explosion, and network degradation are prevented, thereby effectively capturing global and local feature information at each hierarchy. For the structure comparison of the structure of ResNet, Swin Transformer, ConvNeXt, and our HFF blocks, as shown in the figure 3. This process is depicted in (4).

$$\begin{aligned} \text{CA}(x) &= \sigma(\text{MLP}(\text{AvgPool}(x)) + \text{MLP}(\text{MaxPool}(x))) \\ \text{SA}(x) &= \sigma(f^{7 \times 7}(\text{Concat}[\text{AvgPool}(x), \text{MaxPool}(x)])) \\ \text{IRMLP}(x) &= f^{1 \times 1}(f^{1 \times 1}(f^{3 \times 3}(\text{LN}(x)) + \text{LN}(x))) \end{aligned} \quad (4)$$

where σ is the Sigmoid function, $f^{7 \times 7}$ is the convolution operation with a convolution kernel size of 7×7 . The feature fusion operation uses the following formula:

$$\begin{aligned} \hat{G}_i &= \text{CA}(G_i) \otimes G_i \\ \hat{L}_i &= \text{SA}(L_i) \otimes L_i \\ \tilde{F}_i &= \text{Avgpool}(f^{1 \times 1}(x_{f,i-1})) \\ \hat{F}_i &= f^{3 \times 3}(\text{Concat}[G_i, L_i, \tilde{F}_i]) \\ F_i &= \text{IRMLP}(\text{Concat}[\hat{G}_i, \hat{L}_i, \hat{F}_i]) + \tilde{F}_i \end{aligned} \quad (5)$$

where \otimes represents element-wise multiply, \hat{G}_i is generated by the combination of channel attention, \hat{L}_i is generated by the combination of spatial attention, and \tilde{F}_i is generated downsampled by the previous stage of the HFF block. \hat{F}_i is the result of global-local features and the fusion of the previous stage. Finally, \hat{F}_i , \hat{G}_i and \hat{L}_i are concatenated and generate feature F_i through a IRMLP.

4 Experiments

4.1 Dataset

ISIC2018Codella et al. [2019]: We use the ISIC2018 skin lesion diagnosis dataset task 3. There are 10,015 images in this dataset with seven different categories. They are melanocytic nevi (6705), dermatofibroma (115), melanoma (1113), actinic keratosis (327), benign keratosis (1099), basal cell carcinoma (514), and vascular lesions (142). The size of the images in the dataset is 650×450 pixels. We downscale all images to 224×224 pixels and according to the division method of chen[], of which 70% of the samples (7010) are used for training and verification, and the remaining 30% of the samples (3005) are used for testing.

COVID19-CTHe et al. [2020]: This dataset contains 349 COVID-19 positive CT scan images and 397 normal or negative CT scans containing other types of disease. The image sizes in this dataset range from 143×76 to 1637×1225 . We scale all images to 224×224 pixels, follow the data division methodHe et al. [2020] and divide the dataset into a ratio of 0.6:0.15:0.25 for training, validation, and testing.

KvasirPogorelov et al. [2017]: This dataset includes 4000 endoscopic gastrointestinal diseases and comprises eight classes, each containing 500 images. The dataset consists of several images in each category, including anatomical landmarks (such as Z-line, pylorus, or cecum) and pathological findings (such as esophagitis, polyps, or ulcerative colitis). Images with different resolutions from 720×576 to 1920×1072 pixels are included in the dataset. We downscale all images to 224×224 pixels, follow the data division method in literaturePogorelov et al. [2017], and split the dataset into a 50:50 ratio with 2-fold cross-validation.

4.2 Performance Metrics

We choose ACC, F1, Precision, and Recall as classification indicators. These metrics are all calculated based on the confusion matrix. The definitions of the symbols in the confusion matrix are as follows: True Positive (TP), True Negative (TN), False Positive (FP), and False Negative (FN). Therefore, Accuracy (ACC) is calculated by Equation (6) to get the percentage of correctly identified samples.

$$Accuracy = \frac{TP + TN}{TP + TN + FP + FN} \quad (6)$$

Use (7) to calculate the precision rate, the proportion of samples with correct, true values among the samples predicted to be correct, to reflect the accuracy of the model prediction.

$$Precision = \frac{TP}{TP + FP} \quad (7)$$

$$Recall = \frac{TP}{TP + FN} \quad (8)$$

Use (8) to calculate the recall rate, the number of positive samples are found in the data for which all true values are predicted correctly, to reflect the comprehensiveness of the model prediction.

$$F1 = 2 \frac{Precision \times Recall}{Precision + Recall} = \frac{2TP}{2TP + FP + FN} \quad (9)$$

The definition of the F1 score formula for each category is shown in (9). F1 score can solve the balance between precision and Recall, and the higher the value, the better.

4.3 Implementation Details

We selected the SOTA classification model of open-source with similar parameters to HiFuse for comparative experiments [9-12,17,42,43]. We implement our PyTorch-based approach by training on an NVIDIA RTX 3090 GPU with

Table 2: Experimental setting.

training config	224x224
optimizer	AdamW
drop path rate	0
base learning rate	1e-4
min learning rate	1e-6
weight decay	0.01
optimizer momentum	$\beta_1, \beta_2 = 0.9, 0.999$
batch size	32
training epochs	100
learning rate schedule	CosineAnnealing
warm up schedu	linear
warm up epochs	1

24 GB of video memory. The base learning rate value is 1e-4, the batch size is 32, the training epoch is 100, and the cosine annealing learning rate strategy is adopted. To ensure the fairness of the experiments, we use an image size of 224×224, share the same operating environment and hyperparameters, and use the same training, validation, and test sets according to previous literature. We were conducting experiments under the mmcvContributors [2018] framework. We use softmax as the output layer and use the categorical cross-entropy loss function to calculate the loss value:

$$\text{CrossEntropyLoss} = -\frac{1}{N} \sum_{n=1}^N \sum_{i=1}^k y_i^t \log y_i^p \quad (10)$$

where N represents the total number of samples, K represents the number of categories, y_i^t is the target label, and y_i^p is the model’s predicted value output. More parameter settings are shown in Table 2.

4.4 Ablation Study

Table 3: Ablation experiment results on ISIC2018 dataset.

	Acc%	F1%	Prec%	Recall%
Local Path	77.12	54.12	60.03	52.77
+ Global Block	79.59	64.32	64.24	64.66
+ Channel&Spatial Attn	80.85	66.26	69.20	64.60
+ IRMLP	81.32	69.53	72.20	68.28
+Shortcut (HiFuse-Tiny)	82.99	72.99	73.67	72.87

As shown in the Table 3, we evaluated the impact of each component on the model on the ISIC2018 dataset, starting from the local path, adding the global path, channel & spatial attention, Inverted residual MLP, and shortcut, finally, to form the final HiFuse-Tiny model, after adding the global block Acc and F1 increased by 2.47% and 10.2%. After adding components in HFFblock, Acc and F1 increased by 7.4% and 8.67%. It can also be seen that combining the global features can significantly improve the representation ability of the model, and the HFF block can provide a better fusion of global-local features. The above combination achieves an Acc of 82.99% and an F1 value of 72.99%.

4.5 Visual Inspection of HiFuse

To further illustrate that our HiFuse model can effectively capture feature information of medical images, we choose the recent hierarchical structure models ConvNeX-T, Swin Transformer-T, and compare them with our HiFuse-T in this section. We adopt the method of Grad-CAM Selvaraju et al. [2017] to visualize the last layer in the model except for the linear layer and reflect the area of interest in the model in the form of a heat map. Figure 4 (a) and (b) show the Grad-CAM visualization results of some dermoscopy and upper gastrointestinal endoscopy.

As what can be seen, ConvNeX attaches great importance to local features, while Swin Transformer is better at paying attention to global features. The HiFuse model reflects a higher thermal value in the lesion area and more accurately covers the lesion area. Such observations demonstrate that the HiFuse can better integrate global-local features at different levels and helps the model to learn more discriminative features to pay more attention to the lesion area.

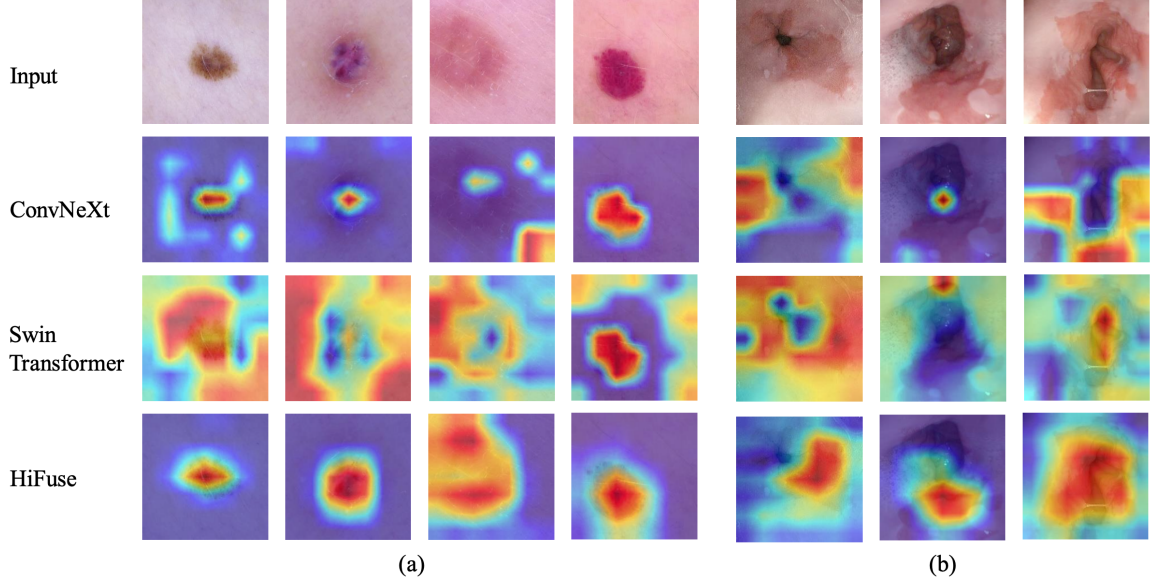


Figure 4: Grad-CAM visual results of ablation experiments.

Table 4: Performance comparison of the ISIC2018 dataset.

Method	Params(M)	Flops(G)	Acc%	F1%	Prec%	Recall%
ConvNeXt-B	88.59	15.36	76.52	50.94	66.84	50.52
VGG-19	143.68	19.67	79.25	61.83	63.71	60.89
Mixer-L/16	208.20	44.57	78.92	59.88	61.36	59.16
T2T-ViT_t-24	64.00	12.69	77.59	57.21	59.60	55.94
DeiT-base	86.57	16.86	72.31	41.01	47.19	44.09
VIT-B/16	86.86	33.03	78.32	60.93	64.16	60.52
Swin-B	87.77	15.14	79.79	63.95	65.09	63.65
VIT-B/32	88.30	8.56	77.92	57.52	58.74	56.90
Conformer-base-p16	83.29	22.89	82.66	72.44	73.31	71.66
HiFuse_Tiny	82.49	8.13	82.99	72.99	73.67	72.87
HiFuse_Small	93.82	8.84	83.59	72.70	72.70	73.14
HiFuse_Base	127.80	10.97	84.12	75.32	76.52	74.74

4.6 Results on ISIC2018 Dataset

Table 4 shows the evaluation results of the proposed model and some advanced classification algorithms on the ISIC2018 dataset. We adopt the data partitioning method in the literature Cheng et al. [2022] and use the initialization network for training.

As what can be seen from the table, HiFuse has significant advantages in medical image classification. Similar to ConvNeXt and Swin Transformer, we build a hierarchical structure to improve the feature representation ability of neural networks of different scales, but 7.6% improves the classification accuracy of our network compared with ConvNeXt and Swin Transformer, respectively (76.52% vs. 84.12%) and 4.33% (79.79% vs. 84.12%). Like Conformer, a multi-branch structure combines the advantages of CNN and Transformer. However, the difference lies in that we do not interact the information of the branches but fuse the branches of the HFF block at different levels to reduce the computational complexity while improving the accuracy of medical image classification.

These experimental results further confirm that the hierarchical fusion of feature information of different branches can reduce the computational complexity and improve the classification model's performance to varying degrees. HiFuse has the above two characteristics. The Flops of HiFuse-Base is only 10.97 G, which has the best classification accuracy (84.12%) on the ISIC2018 dataset.

Table 5: Performance comparison of the Covid19 dataset.

Method	Acc%	F1%	Prec%	Recall%
ConvNeXt-B	55.38	54.68	54.95	54.81
VGG-19	59.14	57.55	59.04	58.13
Mixer-L/16	70.43	70.12	70.38	70.06
T2T-ViT_t-24	63.44	60.34	65.68	61.89
DeiT-base	50.54	39.31	44.47	47.96
VIT-B/16	65.05	64.88	64.90	64.87
Swin-B	60.75	56.36	63.20	58.95
VIT-B/32	61.83	60.59	61.89	60.94
Conformer-base-p16	75.81	75.60	76.81	77.81
HiFuse_Tiny	74.73	74.67	74.65	74.73
HiFuse_Small	76.88	76.31	77.78	76.19
HiFuse_Base	76.34	76.17	76.30	76.11

4.7 Results on Covid19 Dataset

Table 5 shows the evaluation results of the COVID19-CT dataset. We adopt the literature [39] data partitioning method and use the initialization network for training. Among them, the bold represents the best performance.

DeiT-Touvron et al. [2021] has limited classification performance on this dataset. Our analysis for this situation may be that the network structure is mainly designed for large datasets (such as ImageNet) and is not suitable for small datasets such as COVID19-CT. It can be seen from the experimental results that the pure convolutional models ConvNeXtLiu et al. [2022] and VGGSimonyan and Zisserman [2014] are not good at extracting features from small-sample CT datasets, while HiFuse and Conformer using multi-branch network structures have higher classification performance.

HiFuse-Small’s accuracy (76.88%) and F1 value (76.31%) achieved the best performance on this dataset. These results demonstrate that HiFuse can be robust to other applications in the same domain and maintain high classification performance.

4.8 Results on Kvasir Dataset

Table 6: Performance comparison of the Kvasir dataset.

Method	Acc%	F1%	Prec%	Recall%
ConvNeXt-B	74.60	74.61	74.78	74.64
VGG-19	77.75	77.75	77.86	77.83
Mixer-L/16	74.30	74.14	74.43	74.34
T2T-ViT_t-24	76.90	76.78	77.60	76.91
DeiT-base	52.15	48.48	56.72	52.29
VIT-B/16	76.10	75.94	76.49	76.23
Swin-B	77.30	77.29	77.74	77.44
VIT-B/32	73.80	73.50	74.24	73.72
Conformer-base-p16	84.25	84.27	84.45	84.37
HiFuse_Tiny	84.85	84.89	84.96	84.90
HiFuse_Small	85.00	84.96	85.08	85.00
HiFuse_Base	84.35	84.41	84.50	84.48

In order to further explore the generalization ability of HiFuse, we conduct experiments in the Kvasir dataset according to the division method and 2-fold cross-validation in the literature Pogorelov et al. [2017], and the final results are averaged.

It can be seen that HiFuse-Small’s accuracy (85%) and F1 value (84.96%) achieve the best performance in this dataset. Moreover, the accuracy of HiFuse-Base decreases slightly due to the increase in depth, which can be improved slightly by setting the appropriate drop path hyperparameter (the table ensures a fair comparison, not shown). This reminds us that HiFuse-Small with lower depth may have better classification performance when HiFuse is applied to other smaller medical image classification datasets.

In short, capturing global-local features has obvious advantages in medical image classification, and our HiFuse can achieve higher accuracy with lower computational complexity.

5 Discussion

Compared with natural images, medical images have diverse characteristics Zhou et al. [2021], fewer data, and different medical equipment, resulting in limited training data and models that cannot focus well on classification features. Many models that perform well in natural image classification tasks are used in medical image field; satisfactory results cannot be obtained. Therefore, finding an efficient and robust backbone network for medical images remains challenging.

Compared with the convolution operation, Transformer’s self-attention has a global receptive field to mine the long dependencies between pixels, and has a stronger generalization ability. Extensive experiments show that local spatial features are equally important in medical image processing. Based on the above requirements, we design a three-branch hierarchical feature fusion model HiFuse, which fuses global-local feature representations of different scales through the HFF block. In ISIC2018, Covid-19, and Kvasir medical classification datasets, comparison experiments have been conducted to verify that HiFuse has the best results. In addition, our HiFuse benefits from a hierarchical structure with rich scalability, linear computational complexity, and a wider range of applications.

Although our model focused on the task of medical image classification, the ideas presented in this paper can provide researchers with some new ideas for global and local feature fusion. The hierarchical fusion method in the architecture is designed to be easily extended and upgraded.

Our model can be further improved in future research:

1. According to the specific situation of the task, assign the network depth and width of different branches to make the local features and global representation more directional.
2. Design targeted dynamic hierarchical feature selection for different datasets to improve the performance of HiFuse further.
3. Continue HiFuse research in medical image segmentation and multimodal.

6 Conclusion

In this paper, we propose HiFuse, a three-branch hierarchical fusion classification model, and the modular design has rich scalability and linear computational complexity. In HiFuse, the local feature block extracts local features, the global feature block captures global representations, and the hierarchical feature fusion block (HFF block) fuses local features and global representations at different scales, which can comprehensively mine the deep-shallow features and global-local features of the lesion area in the medical image classification task. Experiments show that our proposed method achieves good results on three medical image datasets. We believe this work can contribute to various downstream tasks in medical imagery.

References

- Sven Koitka and Christoph M Friedrich. Traditional feature engineering and deep learning approaches at medical classification task of imageclef 2016. In *CLEF (Working Notes)*, pages 304–317. Citeseer, 2016.
- Yan Xu, Tao Mo, Qiwei Feng, Peilin Zhong, Maode Lai, I Eric, and Chao Chang. Deep learning of feature representation with multiple instance learning for medical image analysis. In *2014 IEEE international conference on acoustics, speech and signal processing (ICASSP)*, pages 1626–1630. IEEE, 2014.
- Wei Shen, Mu Zhou, Feng Yang, Dongdong Yu, Di Dong, Caiyun Yang, Yali Zang, and Jie Tian. Multi-crop convolutional neural networks for lung nodule malignancy suspiciousness classification. *Pattern Recognition*, 61: 663–673, 2017.
- Andre Esteva, Brett Kuprel, Roberto A Novoa, Justin Ko, Susan M Swetter, Helen M Blau, and Sebastian Thrun. Correction: Corrigendum: Dermatologist-level classification of skin cancer with deep neural networks. *Nature*, 546(7660):686–686, 2017.
- L Personnaz, I Guyon, and G Dreyfus. Collective computational properties of neural networks: New learning mechanisms. *Physical Review A*, 34(5):4217, 1986.
- Ashnil Kumar, Jinman Kim, David Lyndon, Michael Fulham, and Dagan Feng. An ensemble of fine-tuned convolutional neural networks for medical image classification. *IEEE journal of biomedical and health informatics*, 21(1):31–40, 2016.
- Yuhai Yu, Hongfei Lin, Jiana Meng, Xiaocong Wei, Hai Guo, and Zhehuan Zhao. Deep transfer learning for modality classification of medical images. *Information*, 8(3):91, 2017.

- Ashish Vaswani, Noam Shazeer, Niki Parmar, Jakob Uszkoreit, Llion Jones, Aidan N Gomez, Łukasz Kaiser, and Illia Polosukhin. Attention is all you need. *Advances in neural information processing systems*, 30, 2017.
- Alexey Dosovitskiy, Lucas Beyer, Alexander Kolesnikov, Dirk Weissenborn, Xiaohua Zhai, Thomas Unterthiner, Mostafa Dehghani, Matthias Minderer, Georg Heigold, Sylvain Gelly, et al. An image is worth 16x16 words: Transformers for image recognition at scale. *arXiv preprint arXiv:2010.11929*, 2020.
- Li Yuan, Yunpeng Chen, Tao Wang, Weihao Yu, Yujun Shi, Zi-Hang Jiang, Francis EH Tay, Jiashi Feng, and Shuicheng Yan. Tokens-to-token vit: Training vision transformers from scratch on imagenet. In *Proceedings of the IEEE/CVF International Conference on Computer Vision*, pages 558–567, 2021.
- Yufei Xu, Qiming Zhang, Jing Zhang, and Dacheng Tao. Vitae: Vision transformer advanced by exploring intrinsic inductive bias. *Advances in Neural Information Processing Systems*, 34:28522–28535, 2021.
- Bangkang Fu, Mudan Zhang, Junjie He, Ying Cao, Yuchen Guo, and Rongpin Wang. Stohisnet: A hybrid multi-classification model with cnn and transformer for gastric pathology images. *Computer Methods and Programs in Biomedicine*, page 106924, 2022.
- Yundong Zhang, Huiye Liu, and Qiang Hu. Transfuse: Fusing transformers and cnns for medical image segmentation. In *International Conference on Medical Image Computing and Computer-Assisted Intervention*, pages 14–24. Springer, 2021.
- Jianyuan Guo, Kai Han, Han Wu, Yehui Tang, Xinghao Chen, Yunhe Wang, and Chang Xu. Cmt: Convolutional neural networks meet vision transformers. In *Proceedings of the IEEE/CVF Conference on Computer Vision and Pattern Recognition*, pages 12175–12185, 2022a.
- Zhiliang Peng, Wei Huang, Shanzhi Gu, Lingxi Xie, Yaowei Wang, Jianbin Jiao, and Qixiang Ye. Conformer: Local features coupling global representations for visual recognition. In *Proceedings of the IEEE/CVF International Conference on Computer Vision*, pages 367–376, 2021.
- Zhuang Liu, Hanzi Mao, Chao-Yuan Wu, Christoph Feichtenhofer, Trevor Darrell, and Saining Xie. A convnet for the 2020s. In *Proceedings of the IEEE/CVF Conference on Computer Vision and Pattern Recognition*, pages 11976–11986, 2022.
- Kaiming He, Xiangyu Zhang, Shaoqing Ren, and Jian Sun. Deep residual learning for image recognition. In *Proceedings of the IEEE conference on computer vision and pattern recognition*, pages 770–778, 2016.
- Ze Liu, Yutong Lin, Yue Cao, Han Hu, Yixuan Wei, Zheng Zhang, Stephen Lin, and Baining Guo. Swin transformer: Hierarchical vision transformer using shifted windows. In *Proceedings of the IEEE/CVF International Conference on Computer Vision*, pages 10012–10022, 2021.
- Sajjad H Baloch and Hamid Krim. Flexible skew-symmetric shape model for shape representation, classification, and sampling. *IEEE transactions on image processing*, 16(2):317–328, 2007.
- Yang Song, Weidong Cai, Yun Zhou, and David Dagan Feng. Feature-based image patch approximation for lung tissue classification. *IEEE transactions on medical imaging*, 32(4):797–808, 2013.
- Junlong Cheng, Shengwei Tian, Long Yu, Chengrui Gao, Xiaojing Kang, Xiang Ma, Weidong Wu, Shijia Liu, and Hongchun Lu. Resganet: Residual group attention network for medical image classification and segmentation. *Medical Image Analysis*, 76:102313, 2022.
- Bichen Wu, Chenfeng Xu, Xiaoliang Dai, Alvin Wan, Peizhao Zhang, Zhicheng Yan, Masayoshi Tomizuka, Joseph Gonzalez, Kurt Keutzer, and Peter Vajda. Visual transformers: Token-based image representation and processing for computer vision. *arXiv preprint arXiv:2006.03677*, 2020.
- Hugo Touvron, Matthieu Cord, Matthijs Douze, Francisco Massa, Alexandre Sablayrolles, and Hervé Jégou. Training data-efficient image transformers & distillation through attention. In *International Conference on Machine Learning*, pages 10347–10357. PMLR, 2021.
- Nicolas Carion, Francisco Massa, Gabriel Synnaeve, Nicolas Usunier, Alexander Kirillov, and Sergey Zagoruyko. End-to-end object detection with transformers. In *European conference on computer vision*, pages 213–229. Springer, 2020.
- Xizhou Zhu, Weijie Su, Lewei Lu, Bin Li, Xiaogang Wang, and Jifeng Dai. Deformable detr: Deformable transformers for end-to-end object detection. *arXiv preprint arXiv:2010.04159*, 2020.
- Josh Beal, Eric Kim, Eric Tzeng, Dong Huk Park, Andrew Zhai, and Dmitry Kislyuk. Toward transformer-based object detection. *arXiv preprint arXiv:2012.09958*, 2020.
- Sixiao Zheng, Jiachen Lu, Hengshuang Zhao, Xiatian Zhu, Zekun Luo, Yabiao Wang, Yanwei Fu, Jianfeng Feng, Tao Xiang, Philip HS Torr, et al. Rethinking semantic segmentation from a sequence-to-sequence perspective

- with transformers. In *Proceedings of the IEEE/CVF conference on computer vision and pattern recognition*, pages 6881–6890, 2021.
- Liang Gao, Hui Liu, Minhang Yang, Long Chen, Yaling Wan, Zhengqing Xiao, and Yurong Qian. Stransfuse: Fusing swin transformer and convolutional neural network for remote sensing image semantic segmentation. *IEEE Journal of Selected Topics in Applied Earth Observations and Remote Sensing*, 14:10990–11003, 2021.
- Hanting Chen, Yunhe Wang, Tianyu Guo, Chang Xu, Yiping Deng, Zhenhua Liu, Siwei Ma, Chunjing Xu, Chao Xu, and Wen Gao. Pre-trained image processing transformer. In *Proceedings of the IEEE/CVF Conference on Computer Vision and Pattern Recognition*, pages 12299–12310, 2021.
- Ziyu Wan, Jingbo Zhang, Dongdong Chen, and Jing Liao. High-fidelity pluralistic image completion with transformers. In *Proceedings of the IEEE/CVF International Conference on Computer Vision*, pages 4692–4701, 2021.
- Jeya Maria Jose Valanarasu, Poojan Oza, Ilker Hacihaliloglu, and Vishal M Patel. Medical transformer: Gated axial-attention for medical image segmentation. In *International Conference on Medical Image Computing and Computer-Assisted Intervention*, pages 36–46. Springer, 2021.
- Xin He, Yushi Chen, and Zhouhan Lin. Spatial-spectral transformer for hyperspectral image classification. *Remote Sensing*, 13(3):498, 2021.
- Yifan Jiang, Shiyu Chang, and Zhangyang Wang. Transgan: Two pure transformers can make one strong gan, and that can scale up. *Advances in Neural Information Processing Systems*, 34:14745–14758, 2021.
- Wenxuan Wang, Chen Chen, Meng Ding, Hong Yu, Sen Zha, and Jiangyun Li. Transbts: Multimodal brain tumor segmentation using transformer. In *International Conference on Medical Image Computing and Computer-Assisted Intervention*, pages 109–119. Springer, 2021.
- Sanghyun Woo, Jongchan Park, Joon-Young Lee, and In So Kweon. Cbam: Convolutional block attention module. In *Proceedings of the European conference on computer vision (ECCV)*, pages 3–19, 2018.
- Jimmy Lei Ba, Jamie Ryan Kiros, and Geoffrey E Hinton. Layer normalization. *arXiv preprint arXiv:1607.06450*, 2016.
- Andrew G Howard, Menglong Zhu, Bo Chen, Dmitry Kalenichenko, Weijun Wang, Tobias Weyand, Marco Andreetto, and Hartwig Adam. Mobilenets: Efficient convolutional neural networks for mobile vision applications. *arXiv preprint arXiv:1704.04861*, 2017.
- François Chollet. Xception: Deep learning with depthwise separable convolutions. In *Proceedings of the IEEE conference on computer vision and pattern recognition*, pages 1251–1258, 2017.
- Saining Xie, Ross Girshick, Piotr Dollár, Zhuowen Tu, and Kaiming He. Aggregated residual transformations for deep neural networks. In *Proceedings of the IEEE conference on computer vision and pattern recognition*, pages 1492–1500, 2017.
- Meng-Hao Guo, Tian-Xing Xu, Jiang-Jiang Liu, Zheng-Ning Liu, Peng-Tao Jiang, Tai-Jiang Mu, Song-Hai Zhang, Ralph R Martin, Ming-Ming Cheng, and Shi-Min Hu. Attention mechanisms in computer vision: A survey. *Computational Visual Media*, pages 1–38, 2022b.
- Noel Codella, Veronica Rotemberg, Philipp Tschandl, M Emre Celebi, Stephen Dusza, David Gutman, Brian Helba, Aadi Kalloo, Konstantinos Liopyris, Michael Marchetti, et al. Skin lesion analysis toward melanoma detection 2018: A challenge hosted by the international skin imaging collaboration (isic). *arXiv preprint arXiv:1902.03368*, 2019.
- Xuehai He, Xingyi Yang, Shanghang Zhang, Jinyu Zhao, Yichen Zhang, Eric Xing, and Pengtao Xie. Sample-efficient deep learning for covid-19 diagnosis based on ct scans. *medrxiv*, 2020.
- Konstantin Pogorelov, Kristin Ranheim Randel, Carsten Griwodz, Sigrun Losada Eskeland, Thomas de Lange, Dag Johansen, Concetto Spampinato, Duc-Tien Dang-Nguyen, Matthias Lux, Peter Thelin Schmidt, et al. Kvadir: A multi-class image dataset for computer aided gastrointestinal disease detection. In *Proceedings of the 8th ACM on Multimedia Systems Conference*, pages 164–169, 2017.
- MMCV Contributors. MMCV: OpenMMLab computer vision foundation. <https://github.com/open-mmlab/mmcv>, 2018.
- Ramprasaath R Selvaraju, Michael Cogswell, Abhishek Das, Ramakrishna Vedantam, Devi Parikh, and Dhruv Batra. Grad-cam: Visual explanations from deep networks via gradient-based localization. In *Proceedings of the IEEE international conference on computer vision*, pages 618–626, 2017.
- Karen Simonyan and Andrew Zisserman. Very deep convolutional networks for large-scale image recognition. *arXiv preprint arXiv:1409.1556*, 2014.

S Kevin Zhou, Hayit Greenspan, Christos Davatzikos, James S Duncan, Bram Van Ginneken, Anant Madabhushi, Jerry L Prince, Daniel Rueckert, and Ronald M Summers. A review of deep learning in medical imaging: Imaging traits, technology trends, case studies with progress highlights, and future promises. *Proceedings of the IEEE*, 109(5):820–838, 2021.